Springer

KSME

Journal of Mechanical Science and Technology 25 (10) (2011) 2519~2528
www.springerlink.com/content/1738-494x
DOI 10.1007/s12206-011-0732-1

Noise and vibration on the bogie of a mass rapid train†

Hsiu-Ying Hwang* and Jia-Shiun Chen

Department of Vehicle Engineering, National Taipei University of Technology, Taipei, Taiwan

(Manuscript Received April 10, 2011; Revised May 5, 2011; Accepted June 17, 2011)

Abstract

This paper investigated a noise and vibration concern on a metro train while the train made turns. The study was conducted to identify the root causes of the vibration and noise through hardware experimental testing as well as dynamic computer simulation. The initial investigation indicated the noise came from the bogie of the train. It was between the slewing ring bearing and the friction sets. A lab test was established to duplicate the reported problem and to root out the causes. One-factor-at-a-time method was used to screen the main key factors. Under certain contact conditions, unsmooth turning would occur and cause the noise and vibration. Dynamic simulation was proposed in the study to predict the potential issue. A multibody dynamic model was built with train body, underbody, slewing ring bearing and friction set to simulate the train turning motion. The results showed unsmooth/discontinuous dynamic motions and torque oscillation behaviors. The stop-and-go and stick-and-slip motion led to the vibration. The analysis confirmed the unsmooth friction forces and adhesion could cause the noise and vibration. The computer simulation showed good correlation with the hardware testing. It demonstrated the computer dynamic simulation could be used to predict the potential friction induced vibration issues. In the study, a different substitute material was also investigated through the computer simulation. The results showed the vibration could be effectively reduced if ceramic compound friction material was used.

Keywords: Noise and vibration; Slewing ring bearing; Bogie noise and vibration; Dynamic simulation; Friction induced vibration; Design of experiments

1. Introduction

Metros are one of the major transportation systems in metropolitan areas. Especially with the rising eco-awareness, saving energy, and reducing emission, more people take metros for their daily commutes. Being safe, affordable, comfortable, convenient, and on-time are the keys to customer satisfaction. In one of the Taipei metro systems, a noticeable noise and vibration were caught attention when trains made turns. The particular trains in the study were unmanned, controlled by the central system with pre-set route, designed accelerations, decelerations and stops. While approaching turns, trains slowed down, and reaccelerated after completing the turns. The noise and vibration occurred during the turns and disappeared after the turns were completed.

Vibration and noise occurred to various transportation systems. Contact condition changes causing the vibration or noise could be commonly seen. Baek et al. [1] studied the transient traction coefficient between the wheel and rail under various conditions. The report showed rolling speed, contact pressure, slip ratio, temperature, relative humidity, and surface roughness and hardness had effects on the traction characteristics. Ohyama [2] studied the adhesion forces between wheel and rails, and found that the changes of contact rigidity affected the traction and slip behaviors. Chen et al. [3] utilized a simplified theory by combining the elasto-hydrodynamic lubrication theory and the contact theory of rough surfaces to analyze the adhesion between wheel and rail. And they found the adhesion coefficient was greatly influenced by the water temperature and asperities height of rough surface. Martins et al. [4] presented and discussed various numerical studies on low speed frictional sliding phenomena. Their work pointed out the effect of static friction to stationary contact and dynamic friction to sliding should be paid distinct attention since static and dynamic friction phenomena were different. Marui et al. [5] investigated the stick-slip vibration using experiments. In their study, the effects to the stick-slip vibration by dynamic friction characteristics, pitching motion, and surface roughness of a slideway were investigated. From the results, it showed the dynamic friction coefficient during the acceleration phase was different from that during the deceleration phase. And a lubricant of small kinematic viscosity was recommended to prevent stick-slip vibration. Mori et al. [6] studied a friction induced vibration on a glass plate. It was found the vibration occurred while the rubbing frequency was close to the natural frequency of the plate. Van De Velde and Baets [7] studied

† This paper was recommended for publication in revised form by Editor Yeon June Kang

* Corresponding author. Tel.: +886 2 2771 2171, Fax.: +886 2 2731 4990
E-mail address: hhwang@ntut.edu.tw

the stick-slip phenomena by observing the relation between the friction force and relative speed. Stick-slip is the phenomenon of unsteady sliding resulting from a varying friction force in combination with elasticity of the mechanical system of which the friction contact is part.

In this paper, study was conducted to identify the root causes of the vibration and noise through hardware experimental testing as well as dynamic computer simulation. The process started with recording the noise on the train, disassembling the systems, and inspecting the condition of each part. A lab test was established to duplicate the reported problem and to root out the causes. Different from the majority of previous researches, a dynamic computer simulation model was created to simulate the condition. The simulation results showed unsmooth/discontinuous dynamic motions and torque oscillations, and predicted the vibration phenomena.

The remaining sections are as follows: an introduction to the metro body bolster and the chassis systems is in Section 2, and followed by the testing set-up, testing results and discussion in Section 3. Section 4 derives the dynamic formulation based on the relative motion of the system and establishes a simulation model to predict the behavior of the system. And finally conclusions are made in Section 5.

2. Systems

The metro train is powered by electricity. Each passenger compartment goes with two bogies. One is located at the front, and the other is at the rear end. The bogie is an assembly providing some flexibility on curves with relative rotation between body and chassis systems. The two bogies act independently. When the train approaches turns, the speed of the train reduces to a pre-set designed value. During turning, the chassis system goes along the direction of the rail. But the body system starts to deviate from the direction where the chassis is heading. The direction of the body is collinear with the centers of the front and rear bogies. The angle between the body and chassis starts small at the beginning of the turn, and gets further apart while the train is further into the turn. Then the angle is gradually reduced when the rail gradually turns back to straight. Finally the body and the chassis are aligned after the turn is completed and the train travels straight.

The relative motion between the train body and chassis is provided by the slewing ring bearing system which is a subsystem of the bogie, as shown in Fig. 1. Fig. 2 shows the slewing ring bearing system. The inner ring of the slewing ring bearing is attached to the body bolster, and the outer ring is to the chassis system, as shown in Fig. 3(a). A pair of friction sets is used to provide resistance to prevent an abrupt relative motion, shown in Fig. 3(b). One of the friction sets is located at the front center, and the other is at the rear center of the bearing.

A friction set includes a rubbing plate, a friction block and a friction block base, as shown in Fig. 4. Two screws/nuts are

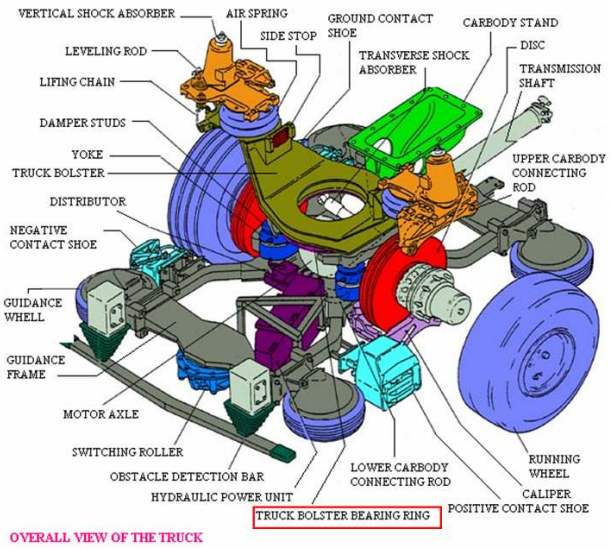

Fig. 1. Body bolster and chassis system.

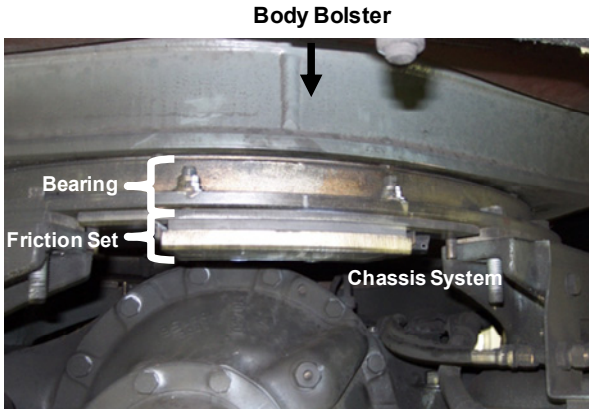

Fig. 2. Bearing system.

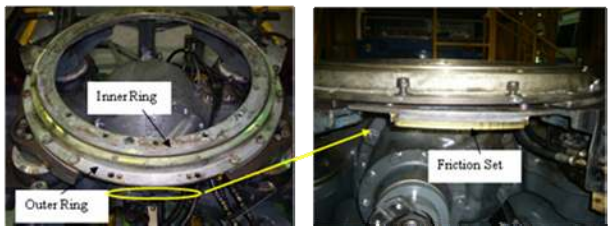

(a) Slewing ring bearing (b) Friction set

Fig. 3. Slewing ring bearing system.

used to press the rubbing plate against the friction block to create the desired contact force and secure the rubbing plate in place. The contact force between the friction block and the rubbing plate provides the resistance during turns. This resistance force prevents the abrupt relative motion between the body and chassis. Fig. 5 shows the contact surfaces of the friction block and rubbing plate.

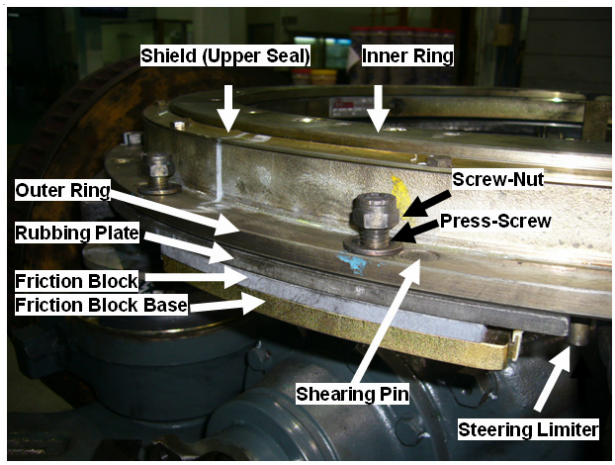

Fig. 4. Components in the bearing system.

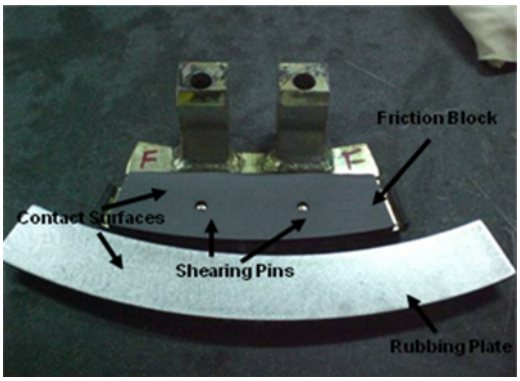

Fig. 5. Contact surfaces between rubbing plate and friction block.

3. Hardware tests

3.1 Process

The investigation process was first done on the train while the train was on its regular duty. Microphones were installed around various underbody of the reported train to record the noise. Noise associated with vibration was observed while the train made turns. After reaching the terminal station, the train was then pulled into the repair bay for further investigation. The repair bay had space and was a good fit for the test without compromising the train schedule or any safety concerns. Both noise and vibration were identified coming from the area between the bearing system and the friction sets with repeated driving on the test track of the repair bay.

The subsystem was disassembled in order to test further in the lab. Lab tests were set-up to duplicate the noise and vibration occurred on the train. The lab test could perform different experiments under a better controllable environment. The set-up was shown in Fig. 6. The lab test focused on the area between the bearing and friction sets. This lab test reduced the complexity of the vehicle-level tests, and the time required for each set-up and changing over.

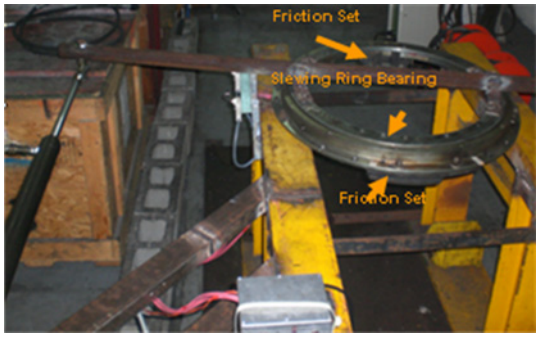

Fig. 6. Lab test.

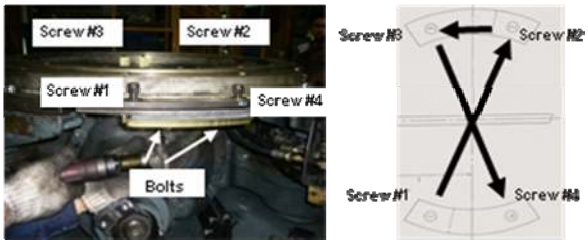

(a) Screw and bolts (b) Sequence of tightening screws

Fig. 7. Screws and bolts on slewing ring bearing.

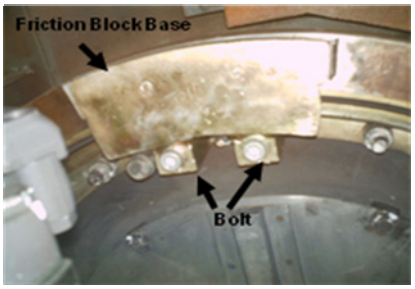

Fig. 8. Bolt from bottom view.

3.2 One factor at a time test

One-Factor-at-A-Time (OFAT) was used to identify the key factors. OFAT [8-11] method investigated each factor individually at a time. It could be easily understood and adopted. The factors chosen for the experimental tests were based on the measurements from the teardown parts and the data recorded on the reported train. The factors were listed below.

(1) Torque of the screws:

The screws secured the rubbing plate to the outer ring to make a tight contact with the friction block, as shown in Fig. 7(a). The screws were secured in two stages. The torque specifications of stages 1 and 2 were 13 Nm and 15.5 Nm, respectively.

(2) Sequence of tightening the screws:

The screws were secured in two stages. During each stage, a

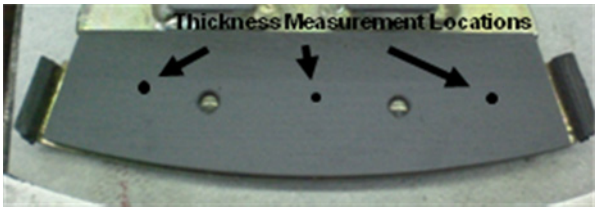

Fig. 9. Locations of friction block thickness measured.

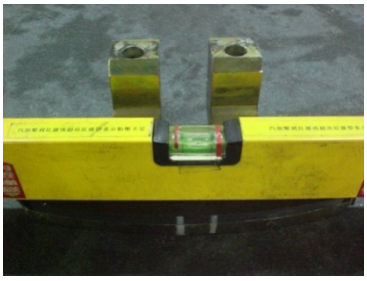

Fig. 10. Warping/deformation check for friction block.

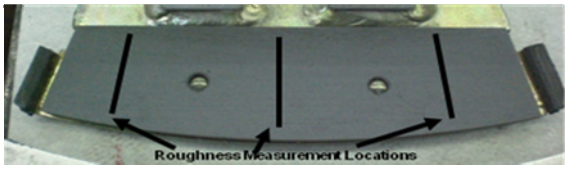

Fig. 11. Locations of friction block surface roughness measured.

defined sequence should be followed, as shown in Fig. 7(b).

(3) Torque of the bolts:

The bolts secured the friction block base to the inner slewing ring, as shown in Fig. 8. The torque specification of the bolts was 135 Nm.

(4) Thickness and uniformity of the thickness of the friction blocks:

The thickness was measured at three locations, as shown in Fig. 9. The nominal thickness of the friction block was 8 mm.

(5) Warping/deformation of the friction blocks:

This check was done on a level check table, as shown in Fig. 10.

(6) Surface roughness of the friction blocks:

Average surface roughness, Ra, was used to measure the surface roughness. Three locations were measured, as shown in Fig. 11.

(7) Thickness and uniformity of the thickness of the rubbing plates:

The thickness was measured at three locations, as shown in Fig. 12. The nominal thickness of the rubbing plate was 8 mm.

Fig. 12. Locations of rubbing plate thickness measured.

Fig. 13. Warping/deformation check for rubbing plates.

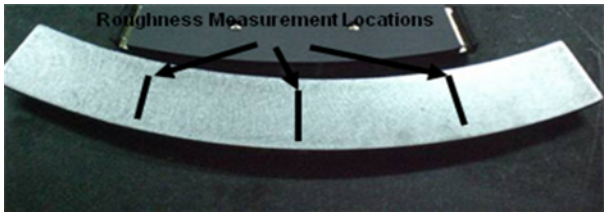

Fig. 14. Locations of rubbing plate surface roughness measured.

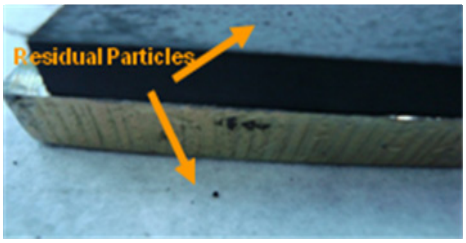

Fig. 15. Residual particles and films.

(8) Warping/deformation of the rubbing plates:

The check was done on a level check table, as shown in Fig. 13.

(9) Surface roughness of the rubbing plates:

Three locations were measured, as shown in Fig. 14.

(10) Residual particles and films:

Residual particles and films between the friction block and rubbing plate were checked, as shown in Fig. 15.

Through the OFAT process, it showed that the factors 1, 2, 4, 7, 8 and 10 had main effects on the vibration/noise of the tested system. The summary was listed in Table 1.

Table 1. One factor at a time test.

ID	Factors	Vibration/Noise
1	Torque of screws	V
2	Sequence of tightening screws	V
3	Torque of bolts	
4	Thickness and uniformity of fiction blocks	V
5	Warping/deformation of friction blocks	
6	Surface roughness of friction blocks	
7	Thickness and uniformity of rubbing plates	V
8	Warping/deformation of rubbing plates	V
9	Surface roughness of rubbing plates	
10	Residual particles and films	V

3.3 Testing results

The factors 1, 2, 4, 7, 8 and 10 had significant effects on duplicating the noise and vibration observed on the train. They were discussed in the following.

For factor 1, when the torque value of the screw was low, the contact force between the rubbing plate and the friction block became low. If the contact force was low, the resistant force became low. Then, the vibration and noise went away. However, without proper contact force, there would be no sufficient force to prevent abrupt relative motion between the body and chassis systems. The torque value of the screws was one of the key controlled processes. Therefore, the frequency of incorrect torque applied to the system was low.

For factor 2, the sequence of tightening the screws affected the torque balance among the 4 screws. The unbalance torque would cause uneven contact between the rubbing plates and friction blocks, and led to the vibration and noise. A two-stage securing sequence was defined to follow. In the first stage, the screws were secured up to 85% value of the torque specification in a sequence shown in Fig. 7. And then, all of screws were tightened to the target torque specification in the same sequence. The sequence of securing the screws was one of the key controlled processes. The frequency of incorrect sequence used was low.

For factor 3, the bolts were used to secure the friction block base to the inner slewing ring. This was done prior the friction plate being secured by the screws, the factor 1. Under the given assembly sequence, factor 3 had little effect on duplicating the vibration and noise condition.

For factors 4 and 7, the uneven distributed thicknesses of the friction blocks and rubbing plates caused uneven contact forces between them. The uneven contact condition became more severe when the un-uniformity of thickness was larger.

For factor 8, the warping/deformation of the rubbing plate affected the contact condition between the rubbing plate and friction block. As the warping of the plate increased, the noise and vibration got more sever. If the warping was bigger than 1 mm, the part was suggested to be replaced. However, for factor 5, due to the high flexibility of the friction block, the warping/deformation of the friction block, had little effect.

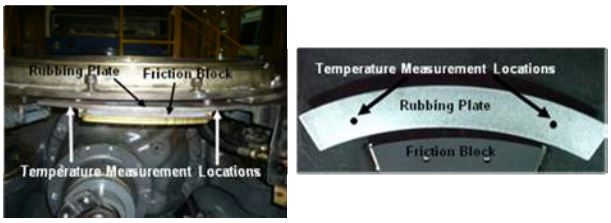

(a) Side view (b) Open view

Fig. 16. Locations of temperature measured.

For factors 6 and 9, the surface roughness of the friction block and the rubbing plate had little effect to the noise and vibration.

For factor 10, the residual particles and films were always found unevenly distributed between the friction block and rubbing plate after several running cycles. The existence of uneven distributed residual particles and films caused un-uniform friction forces between the friction blocks and rubbing plates and led to noise and vibration. If the turning continuously repeated back and forth, the film would get thicker. Because of the friction, the temperature of the contact surfaces got higher, and the film made the friction block and rubbing plate sticky to each other. The residual film was examined. The average value of the dynamic friction coefficient was 0.54. From the friction test, it was noticed that the residual film caused the adhesion between the rubbing plates and the friction blocks when the contact surfaces were rubbed up to the temperature above 150°C. Since the length of the friction block is smaller than that of the rubbing plate, the temperature was measured at the two ends of the rubbing plate contact surface, as shown in Fig. 16. While the friction block moved toward one end of the rubbing plate, the other end of the rubbing plate surface was open up for temperature measurement.

Regular maintenance checks were performed to check the residual particles. The residual particles would be blown off to keep the cleanness of the contact surfaces. Parts with uneven film would be re-processed.

The factors 1, 2, 4, 7, and 8 could be well maintained during the regular maintenance. However, for the 10^{th} factor, the residual particles and films could be formed prior the regular maintenance. For a better result, preventing the particles or films from forming should be the long term solution. Therefore, the following section utilized a dynamic simulation to analyze the behavior caused by factor 10. It predicted the residual particles and films led un-uniform friction forces and sticky condition between friction blocks and rubbing plates.

4. Dynamic simulation

4.1 Derivation – relative motion between inner and outer rings

A dynamic simulation model was created. Fig. 17 was the bogie system modeled in the simulation. It included two

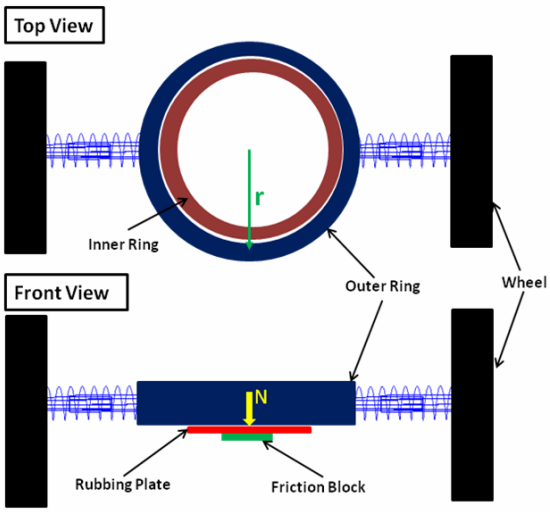

Fig. 17. Turning system.

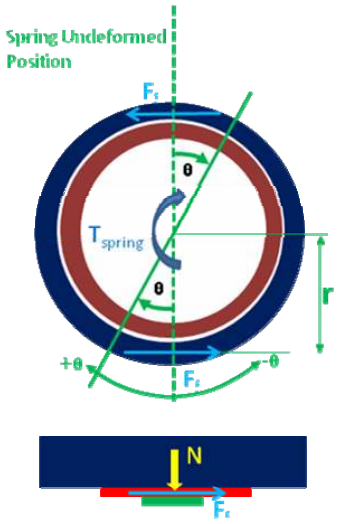

Fig. 18. Free-body diagram.

wheels, two torsion springs and slewing ring bearing system. The slewing ring bearing had inner ring, outer ring, two rubbing plates and two friction blocks. The rubbing plates were attached to the outer ring. One was at the front and the other was at the rear of the outer ring. It's similar for the friction blocks but attached to the inner ring. And the inner ring was attached to the train body. N was a normal contact force pressed on the rubbing plate. And it created a friction force, F_f, between the rubbing plate and friction block, and a friction torque, T_f, with respect to the center of the slewing ring bearing. The effective radius of rubbing plate and friction block to the center of slewing ring was r. A set of torsion springs were placed between the wheels and the outer ring to represent the compliance of the chassis system. The stiffness of the spring was K_O.

On curves, the wheels turned and traveled along the direction of the rail. At the beginning of the turn, the inner and outer rings moved together due to the friction. Let the relative angle between the wheels and outer ring be θ; T_{spring} be the spring torsion torque with respect to the center of slewing ring and act on the slewing ring due to the chassis compliance; and T_f be the friction torque acting on the outer slewing ring from the friction set.

$$T_{spring} = 2K_o\theta \tag{1}$$

$$T_f = 2rF_f \tag{2}$$

where F_f was the friction force. $F_f = N\mu$, and μ was the friction coefficient between the rubbing plates and friction blocks. When $T_{spring} \le T_f$, the inner and outer rings were stuck together. At the moment, the friction torque was due to the static friction forces. The corresponding free-body diagram was shown in Fig. 18. While the wheels kept turning, θ kept increasing till the critical angle, θ_c, and the inner and outer rings were about to slip. Right before the slip,

$$T_{spring} = T_f \tag{3}$$

where $T_{spring} = 2K_o\theta_c$, $T_f = 2rF_f = 2rN\mu_s$, and μ_s was the static friction coefficient. So the following could be obtained:

$$2K_o\theta_c = 2rN\mu_s \tag{4}$$

$$\theta_c = \frac{rN\mu_s}{K_o}. \tag{5}$$

The spring torque was built up and just overcame the static friction torque. The outer ring started to slip. At the moment, the friction force changed and reduced from static to kinetic friction. Let the kinetic friction coefficient be μ_k; the clockwise direction be the positive relative rotation angle between the wheels and outer ring, and counter-clockwise direction be negative; ϕ be the angle traveled from θ_c to θ_f; and θ_f be the final angle when the slip stopped. The system potential energy was dissipated by the friction forces. Based on the principle of work and energy, it could be written as

$$2\left[\frac{1}{2}K_o\theta_c^2 - rF_f\phi\right] = 2\left(\frac{1}{2}K_o\theta_f^2\right) \tag{6}$$

where $\phi = |\theta_c - \theta_f|$. Since ϕ was positive, from Eq. (6), it showed $\theta_c \ge \theta_f$. Thus,

$$\frac{1}{2}K_o(\theta_c^2 - \theta_f^2) = rF_f\phi = rF_f(\theta_c - \theta_f). \tag{7}$$

Since $\theta_c = (rN\mu_s)/K_o$, the following could be derived:

$$\left(\frac{rN\mu_s}{K_o} + \theta_f\right) = \frac{2rF_f}{K_o} = \frac{2rN\mu_k}{K_o} \tag{8}$$

$$\theta_f = \frac{rN(2\mu_k - \mu_s)}{K_o} \tag{9}$$

$$\phi = |\theta_c - \theta_f| = \left|\frac{rN\mu_s}{K_o} - \frac{rN(2\mu_k - \mu_s)}{K_o}\right| = \left|\frac{2rN(\mu_s - \mu_k)}{K_o}\right|. \tag{10}$$

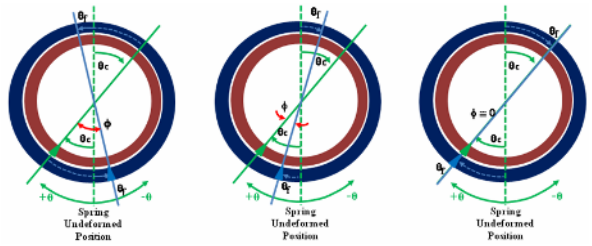

(a) $\mu_s \geq 2\mu_k$ (b) $\mu_s < 2\mu_k$ (c) $\mu_s \cong \mu_k$

Fig. 19. Relative angles.

If $\mu_s \geq 2\mu_k$, from Eq. (9), θ_f was negative. From Eqs. (5) and (10), the following could be derived:

$$\emptyset = \theta_c - \frac{rN(2\mu_k - \mu_s)}{K_o} = 2\theta_c - \frac{2rN\mu_k}{K_o} . \quad (11)$$

From Eq. (11), $\theta_c \leq \phi \leq 2\theta_c$. That meant if the static friction coefficient was more than twice as much as or equal to the kinetic friction coefficient was, then the torsion torque would build up and overcome the friction torque when the wheels continued turning. The outer ring would slip back more than the critical angle, θ_c , and pass the spring undeformed position. The outer ring stayed at a relative angle θ_f to the spring undeformed position, and ϕ to the inner ring. Then the inner and outer rings stuck together again, since the static friction torque became larger than the torsion spring torque. From the critical angle location, the angle the outer ring traveled was between θ_c and $2\theta_c$, as shown in Fig. 19(a).

If $\mu_s < 2\mu_k$, then θ_f was positive, and

$$\emptyset = \theta_c - \frac{rN(2\mu_k - \mu_s)}{K_o} . \quad (12)$$

From Eq. (12), $\phi \leq \theta_c$. That meant if the static friction coefficient was smaller than two times of the kinetic friction coefficient, the outer ring would slip back less than the critical angle, θ_c. The outer ring would stay at a relative angle θ_f to the spring undeformed position, and ϕ to the inner ring. After that, the inner and outer rings stuck together again due to the static friction torque became larger than the torsion spring torque. The total angle traveled, ϕ , was less than θ_c , as shown in Fig. 19(b).

If $\mu_s \cong \mu_k$, then $\theta_f \cong \theta_c$, and $\phi \cong 0$. That meant the inner and outer rings both followed the wheels, but with a constant offset θ_c , as shown in Fig. 19(c).

4.2 Dynamic simulation

An ADAMS multi-body dynamic model, shown in Fig. 20, was built to simulate the causes of the train noise and vibration during the turns. The inner slewing ring was connected with train body. The outer ring was attached to the chassis which was connected with wheels through a set of high torsion stiffness springs. The springs represented the compliance of the chassis structure. A rubbing plate was connected to the outer ring, and a friction block was connected to the inner ring. A friction element was defined between the rubbing plate and the friction block to represent the friction set. An adjustable normal force, N, was applied on the rubbing plate to represent the pressure force between rubbing plate and friction block, as shown in Fig. 21. The friction torque caused by the contact pressure provided the turning resistance torque. The friction coefficient between the friction block and rubbing plate was obtained from the test. The average value of the kinetic friction coefficient was 0.54. From the friction test, it was also noticed that there was residual film built-up in high temperature, above 150°C. The residual film caused the adhesion between the rubbing plate and the friction block. Therefore, a static friction coefficient, 1.0, was used in this dynamic simulation.

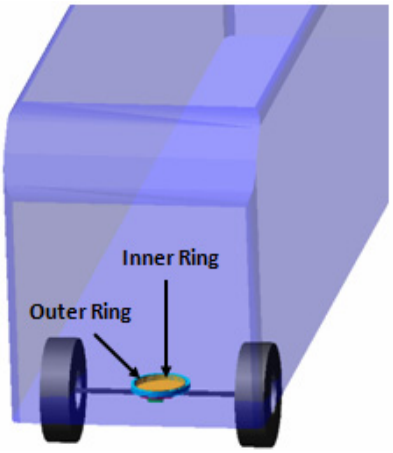

Fig. 20. ADAMS dynamic model.

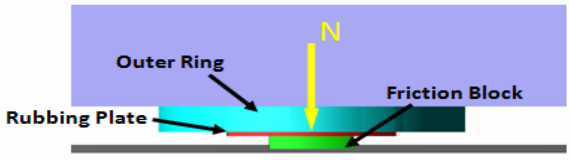

Fig. 21. ADAMS dynamic model for bearing system.

4.3 Simulation results and discussion

A relative rotation motion between the wheels and train body was applied to simulate the wheel turning. Assume the train started with counter-clockwise turn. The wheel had the angular displacement of amplitude of 0.2 and frequency of 0.0318 Hz, $\theta = -0.2 \sin(1/5)t$, where t was time in second. The wheel angular velocity was shown in Fig. 22.

The outer and inner rings were together at the beginning of the wheel turning since the spring torque was smaller than the static friction torque. While the turning went further, the driving spring torque increased and eventually became higher than the static friction torque. And the outer ring abruptly slipped

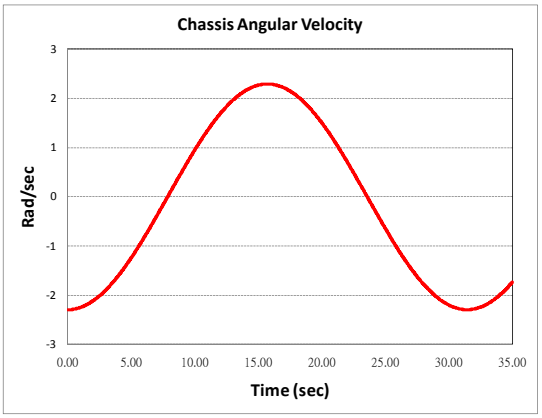

Fig. 22. Angular velocity between wheels and train body.

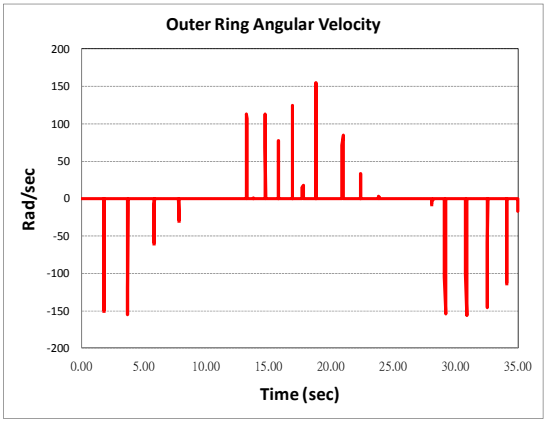

Fig. 23. Relative angular velocity between inner and outer rings.

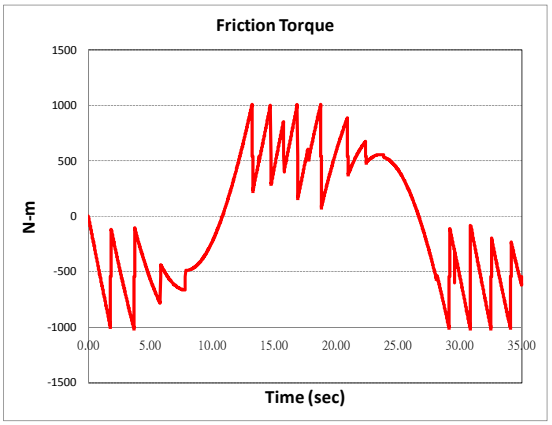

Fig. 24. Friction torque between inner and outer rings.

and rotated relative to the inner ring. After the spring energy was quickly released and dissipated by the friction force, the outer ring stopped rotating relatively to the inner ring. And this motion repeated through the whole wheel turning process, and led several large relative angular velocity impulses as shown in Fig. 23. The highest one could go up to more than 150 rad/sec. This periodic stop-and-go motion could cause

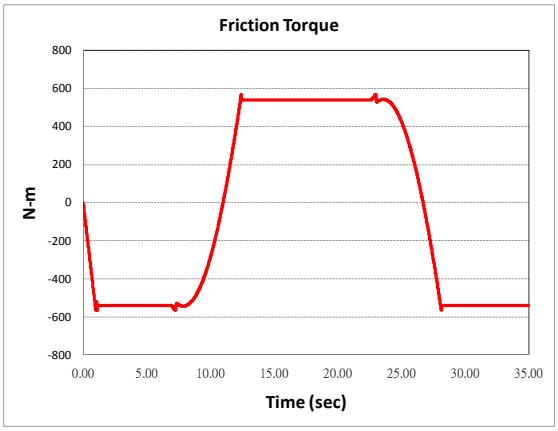

Fig. 25. Friction torque between inner and outer rings (ceramic friction material).

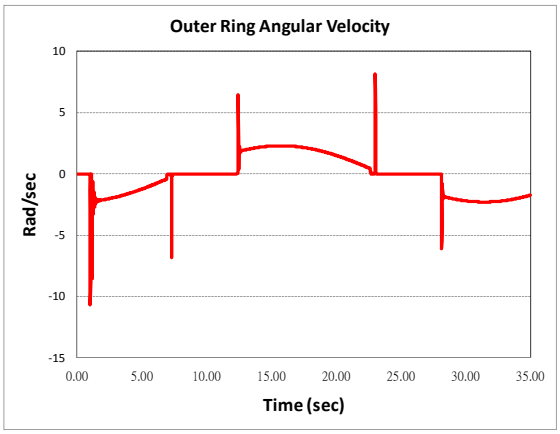

Fig. 26. Angular velocity between inner and outer rings (ceramic friction material).

vibration and noise at the outer ring and the parts connected to it. The fluctuation of friction torque between the inner and the outer rings could be seen through the whole wheel turning process as shown in Fig. 24. It's in sync with each velocity change and the stop-and-go motion. The phenomenon confirmed the initial investigation that the vibration/noise came from the slewing bearing system. It happened when the friction set was heated-up after a period of running hours. The residual particles and films were the side products of the friction set from repeated rubbing. They created adhesion, high stickiness and caused un-uniform friction forces and torques during the turning motion.

Regular maintenance was used to check the residual particles or films. Different types of material for the friction blocks were investigated. A ceramic compound matrix with copper fiber was identified as a potential substitute for the original neoprene rubber. The ceramic compound had stable and predictable friction characteristic. It's commonly used in brake systems. It provided stable braking performance without generating sticky residual films. The material itself also had damping features that would help in diminish some noise and

vibration. The average value of its kinetic friction coefficient was around 0.4, even the temperature of the contact surfaces became high due to repeated surface rubbing. The normal contact forces between the rubbing plates and friction blocks were adjusted to maintain the same resistance torque as before. A dynamic simulation was performed with the same setting and wheel angular displacement, but a static friction coefficient of 0.42, and the kinetic of 0.4. The analysis results were shown in Figs. 25-26. Fig. 25 showed no oscillation in the friction torque curve. The positive and negative friction torques were due to the rotation direction changes while wheel turned left and right. Fig. 26 showed the relative angular velocity between the inner and the outer rings. The relative angular velocity remained small all the time except several peaks. The first peak was to overcome the static friction force from rest. The peak around 7.8 sec and the one next to it were due to wheels turning from left to right and its torque build-up. Similarly to the peak around 23.6 sec and the one next to it, this time was due to the wheels turned to left. All the peaks had values less than 11 rad/sec, and were much smaller than the original friction block with peak of 150 rad/sec in Fig. 23. This new proposed friction block material would not expect to have a similar friction induced noise and vibration.

5. Conclusions

The studies were conducted to identify the root causes of the vibration and noise on metro underbody through hardware testing as well as dynamic computer simulation. A lab test was established to duplicate the reported problem. The noise associated with vibration occurred when the train made turns. And they went away after the turns were completed.

The study investigated ten factors using one-factor-at-a-time method to identify the key factors. This method could be easily understood and adopted for key factor screening process. Six of them were identified critical to the reported noise and vibration condition. The six key factors are:

- torque values of the screws which secured the rubbing plates to the outer slewing ring,
- sequence of tightening the screws,
- thickness and uniformity of the thickness of the friction blocks,
- thickness and uniformity of the thickness of the rubbing plates,
- warping/deformation of the rubbing plates,
- residual particles and films between the friction blocks and the rubbing plates.

From the lab tests, unsmooth turning motion was observed and led to noise and vibration. A corresponding maintenance procedure was suggested according to the findings in the study. When necessary, part replacement would be made. The residual film, the last factor in the list, was further studied for a long term solution. It was found that the residual film caused the adhesion between the rubbing plates and the friction blocks when the contact surfaces were rubbed up to a temperature above 150°C. A dynamic simulation was proposed to investigate the behaviors caused by the residual film.

A multibody ADAMS dynamic analysis model was built with train body, underbody, slewing ring bearing and friction set to simulate the train turning motion. The simulation results showed the residual particles/films caused unsmooth and discontinuous dynamic motions, and torque oscillations. It was a stop-and-go and stick-and-slip motion, and led to the vibration. The analysis confirmed the unsmooth friction forces and adhesion caused the noise and vibration. Computer simulation showed good correlation with the hardware testing. It demonstrated dynamic computer simulation could be used to predict the potential friction induced vibration issues.

In the study, a different substitute material was also investigated through the computer simulation. A potential substitute, ceramic compound material, for the friction block was simulated. Based on the simulation results, the vibration phenomenon could be effectively reduced if ceramic compound friction material was used.

Nomenclature

ϕ	: Angle traveled
μ	: Friction coefficient
μ_k	: Kinetic friction coefficient
μ_s	: Static friction coefficient
θ	: Relative angle between wheel and outer ring
θ_c	: Critical angle
θ_f	: Final angle
r	: Effective radius of rubbing plate/friction block to the center of slewing ring
t	: Time
K_o	: Stiffness of torsion spring
F_f	: Friction force
N	: Normal contact force
T_f	: Friction torque
T_{spring}	: Spring torsion torque

References

[1] K. -S. Baek, K. Kyogoku and T. Nakahara, An experimental study of transient traction characteristics between rail and wheel under low slip and low speed conditions, *Wear,* 265 (2008) 1417-1424.

[2] T. Ohyama, Tribological studies on adhesion phenomena between wheel and rail at high speeds, *Wear,* 144 (1991) 263-275.

[3] H. Chen, T. Ban, M. Ishida and T. Nakahara, Adhesion between rail/wheel under water lubricated contact, *Wear,* 253 (2002) 75-81.

[4] J. A. C. Martins, J. T. Oden and F. M. F. Simões, A study of static and kinetic friction, *Int. J. Engng Sci.,* 28 (1) (1990) 29-92.

[5] E. Marui, H. Endo, M. Hashimoto and S. Kate, Some considerations of slideway friction characteristics by observing

stick-slip vibration, *Tribology International,* 29 (3) (1996) 251-262.
[6] H. Mori, O. Mikhyeyev, T. Nagamine, M. Mori and Y. Sato, Effect of a dynamic absorber on friction-induced vibration of a rectangular plate, *Journal of Mechanical Science and Technology,* 24 (2010) 93-96.
[7] F. Van De Velde and P. De Baets, The relation between friction force and relative speed during the slip-phase of a stick-slip cycle, *Wear,* 219 (1998) 220-226.
[8] D. Montgomery, *Design and analysis of experiments*, Wiley, New York, USA (1997).
[9] D. Besterfield, *Quality control*, Pearson Prentice Hall, New Jersey, USA (2004).
[10] K. Ranjit, *Design of experiments using the taguchi approach: 16 steps to product and process improvement*, John Wiley & Sons, New York, USA (2001).
[11] G. Box, W. Hunter and J. Hunter, *Statistics for experimenters*, Wiley, New York, USA (1978).

Hsiu-Ying Hwang received her Ph.D degree in Mechanical Engineering from the University of Iowa, Iowa City, USA. She is an assistant professor in the Department of Vehicle Engineering, National Taipei University of Technology, Taipei, Taiwan. Her researches include vehicle design, optimization, vehicle NVH, solid mechanics, finite element methods, and 6-sigma quality control.

Jia-Shiun Chen received his Ph.D degree in Mechanical Engineering from the University of Iowa, Iowa City, USA, and is an assistant professor in the Department of Vehicle Engineering, National Taipei University of Technology, Taipei, Taiwan.